The Hydrodynamic Characteristics Induced by Multiple Layouts of Typical Artificial M-Type Reefs with Sea Currents Typical of Liaodong Bay, Bohai Sea

Shu, A., Rubinato, M., Qin, J., Zhu, J., Sun, T., Yang, W., Wang, M. & Zhang, Z.

The Hydrodynamic Characteristics Induced by Multiple Layouts of Typical Artificial M-Type Reefs with Sea Currents Typical of Liaodong Bay, Bohai Sea

Anping Shu [1,*]**, Matteo Rubinato** [2]**, Jiping Qin** [1,3]**, Jiapin Zhu** [1]**, Tao Sun** [1]**, Wei Yang** [1]**, Mengyao Wang** [4] **and Ziyue Zhang** [1]

1 School of Environment, Key Laboratory of Water and Sediment Sciences of MOE, Beijing Normal University, Beijing 100875, China; 201821180006@mail.bnu.edu.cn (J.Q.); 202021180067@mail.bnu.edu.cn (J.Z.); suntao@bnu.edu.cn (T.S.); yangwei@bnu.edu.cn (W.Y.); 201821180058@mail.bnu.edu.cn (Z.Z.)
2 Centre for Agroecology, Water and Resilience, School of Energy, Construction and Environment, Coventry University, Coventry CV1 5FB, UK; matteo.rubinato@coventry.ac.uk
3 Environmental Planning Research Center, Yunnan Research Academy of Eco-Environmental Sciences, Kunming 650034, China
4 Beijing Water Resources Dispatching Center, Beijing 100038, China; 201721180007@mail.bnu.edu.cn
* Correspondence: shuap@bnu.edu.cn; Tel.: +86-135-0117-6507

Abstract: Artificial reefs are effective measures to improve the marine ecological environment and increase fishery production. However, there are several geometries being investigated nowadays and their setup, including the spacing between groups of them, can provide dissimilar effects on hydrodynamics. To enhance the understanding of this topic, in this paper, the focus is mainly on M-Type artificial reefs that will be adopted in Juehua Island, Liaodong Bay, China. An experimental campaign was carried out in order to simulate the influence that M-Type unit reef groups may have on the local flow field and the Particle Image Velocimetry (PIV) technique has been implemented to provide velocity maps. The results showed that with the increase of velocity's current approaching the artificial reef, the height, length and area of the upwelling and the back vortex rise with the increase of spacing between the artificial reefs. Furthermore, when comparing different geometrical configurations with similar currents approaching the artificial reef, the maximum values of both upwelling and back vortex were obtained when the spacing between unit reefs was 1.25 L. Finally, the entropy method was used to evaluate the effects on the flow field under four kinds of spacing based on the hydrodynamic characteristics and the economic cost. The comprehensive score obtained for all the configurations followed the order 1.25 L > 1.50 L > 0.75 L > 1.00 L. Therefore, it is suggested that the original design spacing should be increased by 25% when the M-type unit reef is put into practice. Additionally, after having completed a comparative analysis, it is recommended to further change the reef group into four reef monocases. By executing this adjustment, the unit reef cost was reduced by 10%, and the influence range on the flow field increased by 10%, and this result can consequently achieve greater ecological benefits with less economic input. The results of this study provide a preliminary reference for the construction of artificial reefs M-Type from the perspective of theory and practice.

Keywords: artificial reef; PIV experiment; flow field; hydrodynamics; entropy method

1. Introduction

In recent years, due to the pollution of offshore environments, habitats' degradation, overfishing and climate change, global marine fishery resources have declined significantly [1–4]. To re-establish a sustainable equilibrium, countries across the world have adopted the use of artificial reefs, which are considered to be an effective measure to reduce the impact of human activities on coastal ecosystems and increase fishery production, and have flourished as a result [5,6]. These are defined as "submerged structure[s] deliberately

constructed or placed on the seabed to emulate some functions of a natural reef, such as protecting, regenerating, concentrating, and/or enhancing populations of living marine resources, hence providing ecological benefits" [7,8]. When locating artificial reefs into marine environments, it is well researched that they tend to generate blocking effects to existing currents. More in detail, currents approaching towards them are usually split into two parts, one uplifted to form upwelling, and another which passes through the reef and produces eddy and sedimentary currents [9]. The upwelling current can promote the exchange between the upper and lower layers of the seawater, increase the transport of nutrients within the bottom and top layers. In fact, due to the presence of the artificial reef, a gentle and stable eddy current characterized by low velocity is indeed generated on the back of the reef, which facilitates the deposition of nutrients, and provides a place for fish and other organisms to live, avoid enemies and feed, therefore enhancing fish gathering. These characteristics then tend to enhance the presence of fish which is attracted by the high quantities of nutrients to feed on plankton or smaller fish, attracting other predators in the nearby locations [10–19]. Therefore, due to this impact that artificial reefs can have on flora and fauna in marine environments, it is essential to evaluate, assess and determine with precision which flow field generates and what are the effects they cause, being vital and crucial for the fate of marine environment [20–24].

To date, the most common methods to investigate the hydrodynamic characteristics of artificial reefs relate to numerical simulations or experimental tests conducted within wind tunnel or flumes, where particle image velocimetry (PIV) techniques can be applied [25–31]. Previous studies conducted by adopting these methods have highlighted a list of factors that can alter the hydrodynamic characteristics of artificial reefs, and this includes the original flow field and the existing terrain, the location of the new artificial reefs placed, the manufacturing materials, the shape and the structure, the opening ratio and the upstream area of the reefs, as well as the number of elements [32–38]. Most of the studies available in literature refer to single artificial reefs, however, when these are implemented within marine regions across the world, their setup involves groups of them which form proper reef belts, and there is a need to accurately assess the performance of them as a full unit rather than their independent performance. Therefore, more attention should be paid to the hydrodynamic effects caused by larger scale reefs.

The spacing between reefs is indeed an important factor affecting the flow field between, before and after unit reefs. Yu et al. [39] studied the effect that various artificial reef arrangements may have on hydrodynamic characteristics by conducting both experimental tests within a flume and by completing numerical simulations too. The results showed that the scale and the resistance coefficient of the rising flow of the two reefs are inversely proportional to the vertical flow layout spacing, and that the rising scale is directly proportional to the distance of the parallel flow. Guan et al. [40] used numerical simulations to study the influence of spacing within three tube artificial reefs. The results showed that when the spacing is arranged according to the size of the reefs, the maximum values and strengths of the upwelling and the back vortex can be obtained. Furthermore, the effect on flow field had bigger magnitude when the longitudinal distance between reefs was 1.5~2.0 times the reef's size. Pang et al. [41] simulated the three-dimensional flow field of porous hollow composite reef with the same air permeability under three kinds of reef spacing by adopting CFD technology, and found that the scale and intensity of the upwelling firstly increased and then decreased with the increase of the reef spacing, and the flow field effect was more mild when the reef spacing was twice the reef length. Although there are many studies on the influence of layout spacing on the flow field generated by artificial reefs, most of the studies at this stage focus on maximum two individual reefs, and there is a lack of research on the layout spacing of unit reefs and other large scales. Additionally, the available studies are mostly descriptive, based on observations and there is a need for more experimental and numerical studies to estimate the strength and scale of upwelling and back vortex currents induced by various unit reefs spacing to aid the development and stipulation of design guidelines for local and national authorities.

To fill this gap, in this study, units of M-type reefs, to be planted in the typical artificial reefs area of Bohai Bay, were selected as the research objects. These M-shaped reefs have been proposed by local authorities for the protection of coastal environment in Liaodong Bay. In literature there are other shapes that to date have been presented such as hollow cubes, B-plus shape, pentagon dome, octpus and multi holes [36] and considering all the implications that artificial reefs may have once located, it has been necessary to start to investigate the effects that these M-shaped reefs may have as well. Therefore, dissimilar internal spacing between these unit reefs was tested and the particle image velocimetry (PIV) technology was applied to quantify the flow fields generated for each scenario. The experimental facility was developed to carry out, in a multi-function tank, simulations to replicate oceanic conditions, to explore the influence of spacing on the flow fields linked with each different unit reef. At the same time, the entropy method was used to evaluate the experimental results, in order to provide a reference for the selection of unit reef spacing and reasonable layout of reefs.

2. Methodology

2.1. Artificial Reef Model

The reef monocase model with holes of 400 mm inclined by 41° is displayed in Figure 1. The dimensions adopted were considered by applying the geometric factor of 1:50 according to the prototype size of M-type Reef. Applying the principles of the Froude Similitude, the models were made of plexiglass. Each M-type unit reef is composed of 14 reef monocases, organized in three groups, 4 in the front part, 4 at the back and 6 in the middle. In order to avoid drifting and rolling of the artificial reefs, the models were fixed at the bottom of the flume with transparent rubber belts and were positioned perpendicularly to the flow direction.
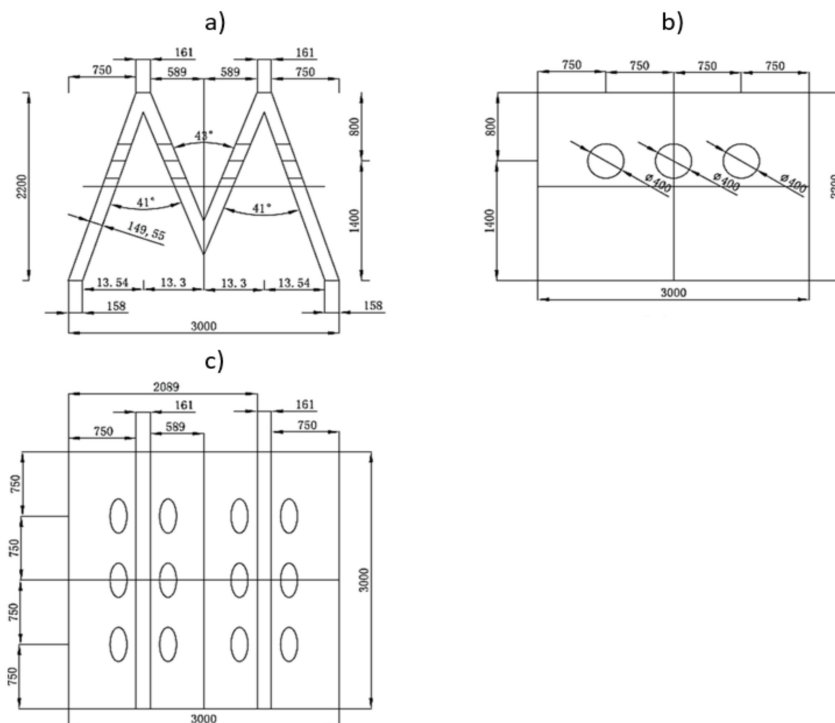

Figure 1. (**a**) Lateral, (**b**) side and (**c**) aerial views of the artificial reef prototype tested (all dimensions in mm).

2.2. Experimental Setup

The experimental campaign was carried out in a multi-functional circulating flume in the State Key Laboratory of Water Environment Simulation, at Beijing Normal University,

China. The internal dimensions of the flume are 25.00 m × 0.80 m × 0.80 m (length × width × height), whose bottom and sides are made of transparent glass to facilitate the observation of hydraulic phenomena. The flow was generated by a complete water circulation system, and the maximum flow rate tested was 240 L/s. The experimental setup is illustrated in Figure 2.
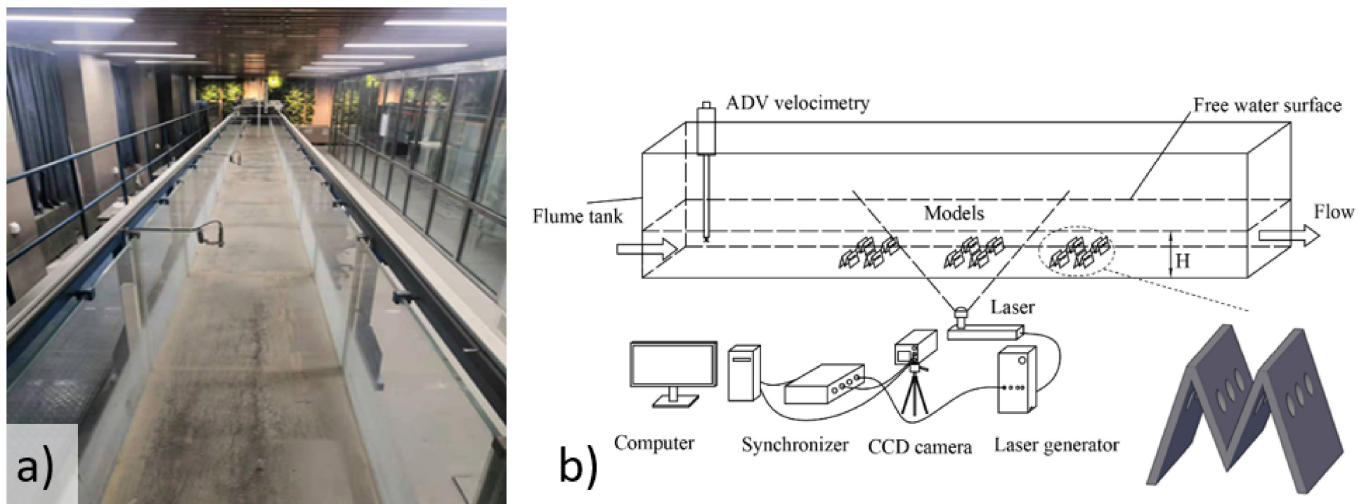

Figure 2. (**a**) Upstream view of the experimental facility, (**b**) schematic diagram of the experimental flume and setup and 3D representation of M-Type artificial reefs implemented.

The facility was setup to enable the application, as previously mentioned, of a PIV system. More in detail, this is a non-contact two-dimensional flow field measurement technology based on cross-correlation analysis of flow field images, which can produce flow maps and instantaneous flow patterns. It is usually adopted and applied to support the development of models for complex flows or validation of numerical simulations. Nowadays, it has become one of the main experimental technique for measuring velocity fields [42–48] and has been widely used in the analysis of flow fields around artificial reef models in recent years [49,50].

To setup the experimental facility to enable the application of this technique, an Acoustic Doppler Current Velocimetry (ADV) was installed 1~2 m in front of the test target to measure the inflow velocity. The artificial reef model was placed in the middle of the flume. The laser was placed at the bottom of the tank so that it could hit the central axis of the reef model. The instantaneous frames were recorded by a CCD camera for 5 min and then were analysed by using Dynamic Studio software. The results of the velocity were then finally visualised using Tecplot software.

2.3. Boundary Conditions

In the real case scenario, along the flow direction, the spacing between each reef monocases group is 18.85 m, which corresponds to 377 mm (L) in the flume experiment according to the Froude Similitude adopted. On this basis, the spacing was reduced and expanded as trials to verify consequent effects, and four different spacing and a reef free control group were set up, which were $L_1 = 0.75\ L = 283$ mm, $L_2 = 1.00\ L = 377$ mm, $L_3 = 1.25\ L = 471$ mm, $L_4 = 1.50\ L = 566$ mm, respectively. According to Cui et al., [51], the best spacing between the two reef monocases should be 1~1.5 times the length of the reef. Therefore, the spacing between two monocases in each group was set up as one time of model length, that was, 60 mm. The specific placement form is shown in Figures 3 and 4.
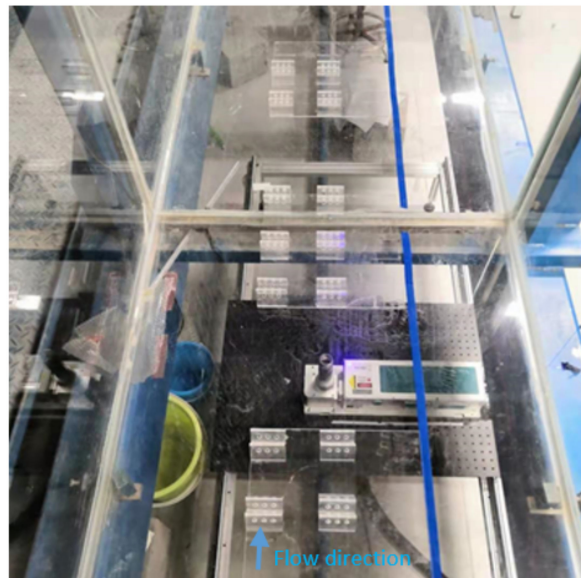
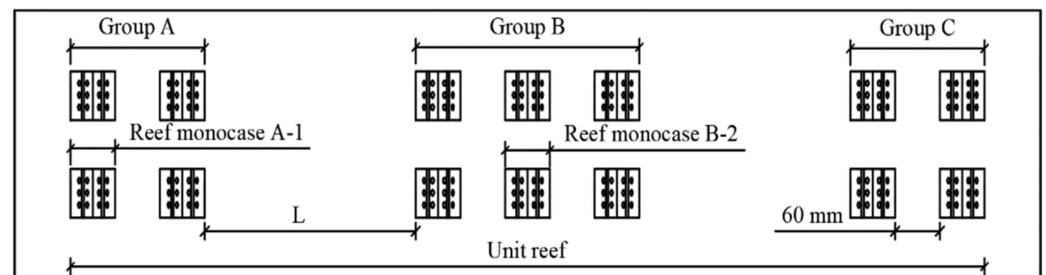**Figure 3.** Aerial view of the artificial reefs placement.

Figure 4. Composition of the reefs in the flume.

The experimental velocity (u_0) tested within this study was calculated according to the maximum velocity of the sea currents in the area where artificial reefs are placed. Five velocities recorded in the sea area of Juehua Island, where the M-type reefs will be launched, were selected, which are 0.6 m/s, 0.9 m/s, 1.2 m/s, 1.5 m/s and 1.8 m/s [52–55]. Based on the Froude Similitude, the correspondent experimental velocities to be tested in the lab resulted to be 0.085 m/s, 0.130 m/s, 0.170 m/s, 0.214 m/s and 0.257 m/s.

The experimental water depth was kept at 300 mm, and this value was calculated according to the actual water depth recorded at sea around Juehua Island, which corresponded to 15 m. Prior to each test, the water tank gradient was constant, and the experimental conditions were achieved by adjusting the angle of the flowmeter and the tailgate. The flow was let stabilize for 5 min and then the velocity measurement were gathered for 5 min. To sum up, a total of 25 groups of experiments were conducted, as shown in Table 1. No wave condition was applied.

Table 1. Test conditions.

Experimental Group (Test Case)	L (mm)	u_0 (m/s)	Q (L/s)
0 (1–5)	\	0.085	20
1 (1–5)	283	0.13	30
2 (1–5)	377	0.17	40
3 (1–5)	471	0.214	50
4 (1–5)	566	0.257	60

Note: L: the internal spacing of artificial reef group, u_0: the average velocity of incoming flow, Q: the flow rate.

3. Results

3.1. Laws of the Velocity Ditribution in Artificial Reef Areas

Effects on the flow field generated by the presence of artificial reefs were mainly observed in the upwelling area in front of the reefs and behind the reefs, where a back vortex condition was noticed. Therefore, the distribution of the upwelling and the back vortex around the reefs were mainly considered when analyzing the hydrodynamic characteristics of artificial reefs [56].

3.1.1. Experimental Settings for Analysis

In order to accurately compare the changes of longitudinal and vertical velocity under different velocity conditions, 16 cross-sections were identified as displayed in Figure 5. More in detail, Section A and Section B are 60 mm (1 times reef length) and 30 mm (1/2 times reef length) before the first group (Group A, as introduced in Figure 5) of artificial reefs; Section C is 30 mm after the first monocase of Group A; Section D, Section E and Section F are 30, 60 and 120 mm after the last monocase of Group A; Section G, Section H, and Section I are 120, 60, and 30 mm in front of the second group of artificial reefs, Group B; Section J is 30 mm after the first monocase in Group B; Section K is 30 mm after the second monocase in Group B; Section L is 30 mm after Group B; Section M is 30 mm before the final group of artificial reefs, Group C; Section N is 30 mm after the first monocase in Group C; Section O and Section P are 30 mm and 60 mm after Group C.
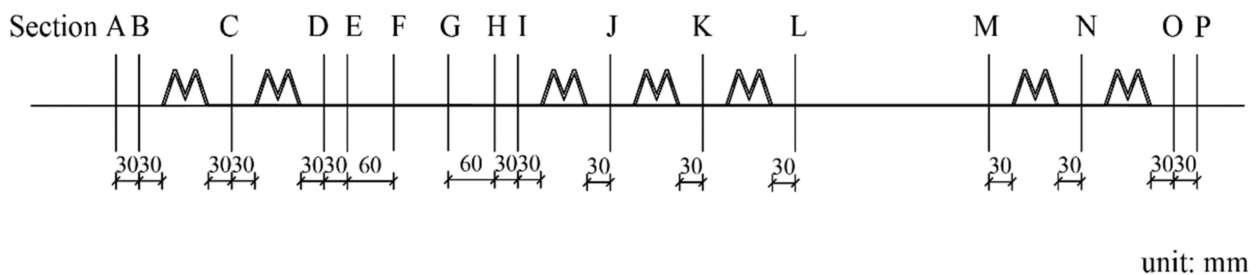
Figure 5. Settings of the cross-section in the artificial reef area.

3.1.2. Longitudinal Velocity Distribution

According to the location of these sections relative to the unit reefs, the 16 sections are classified into four categories as follows:

- A and B are the sections not entering the reef area (Type I);
- D, E, F, L, O, and P are the rear sections of the reef groups (Type II);
- C, J, K, and N are the sections between the two reef monocases (Type III);
- G, H, I, and M are the front sections of the reef groups (Type IV).

Taking the flow velocity of 0.130 m/s as an example, the longitudinal velocity distribution of each section under different spacing is compared and analyzed. The specific relationship between longitudinal velocity and relative water depth H_r (H/h, water depth/reef height) are shown in Figure 6.

Figure 6. *Cont.*

Figure 6. Longitudinal velocity distribution of each section of M-shaped unit reef.

(1)   Type I

Because it is hardly affected by the reef groups, the longitudinal velocity distribution of Sections A and B not in the artificial reef area conforms to the logarithmic distribution law which can be fitted with Equation (1), R^2: 0.99.
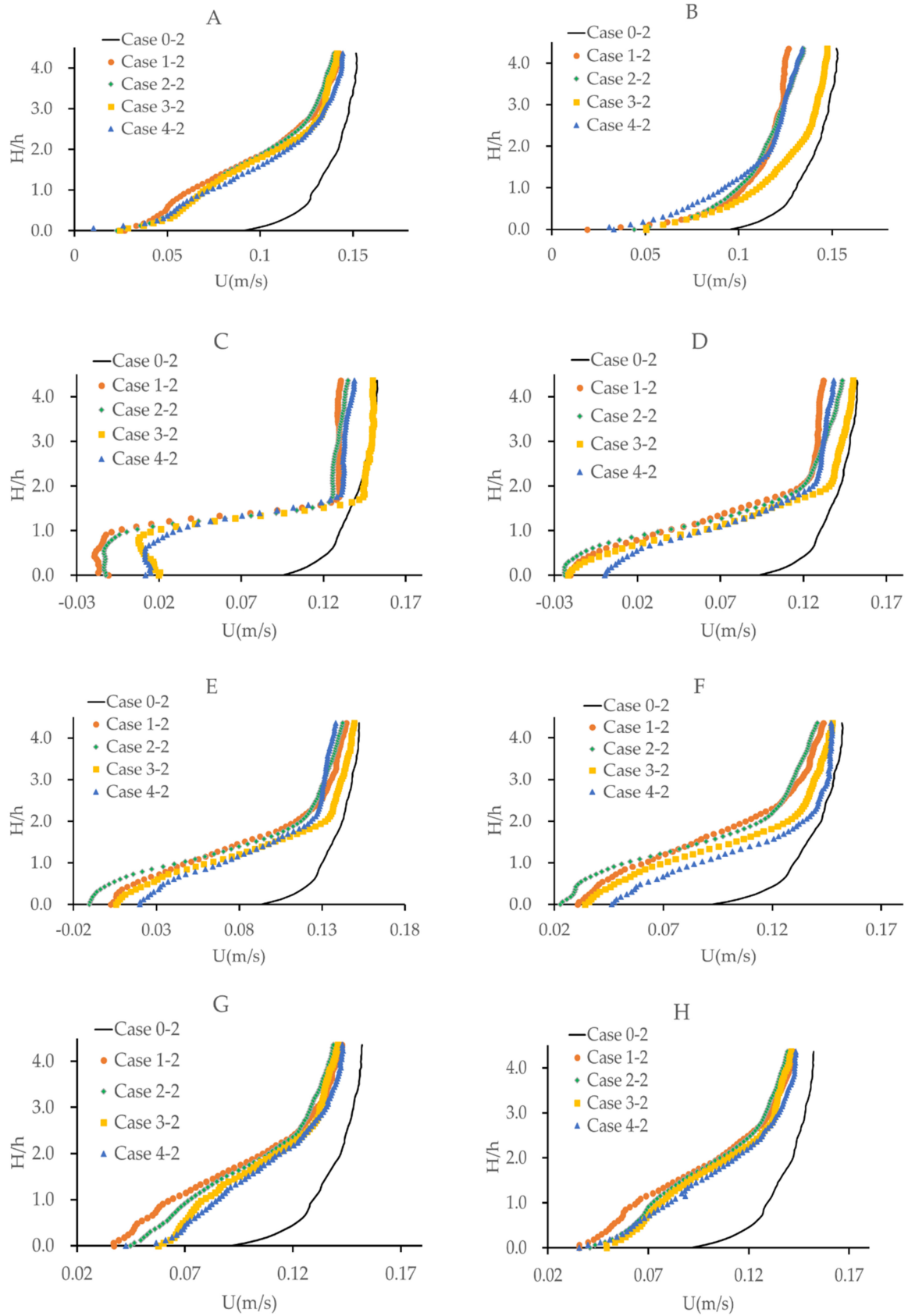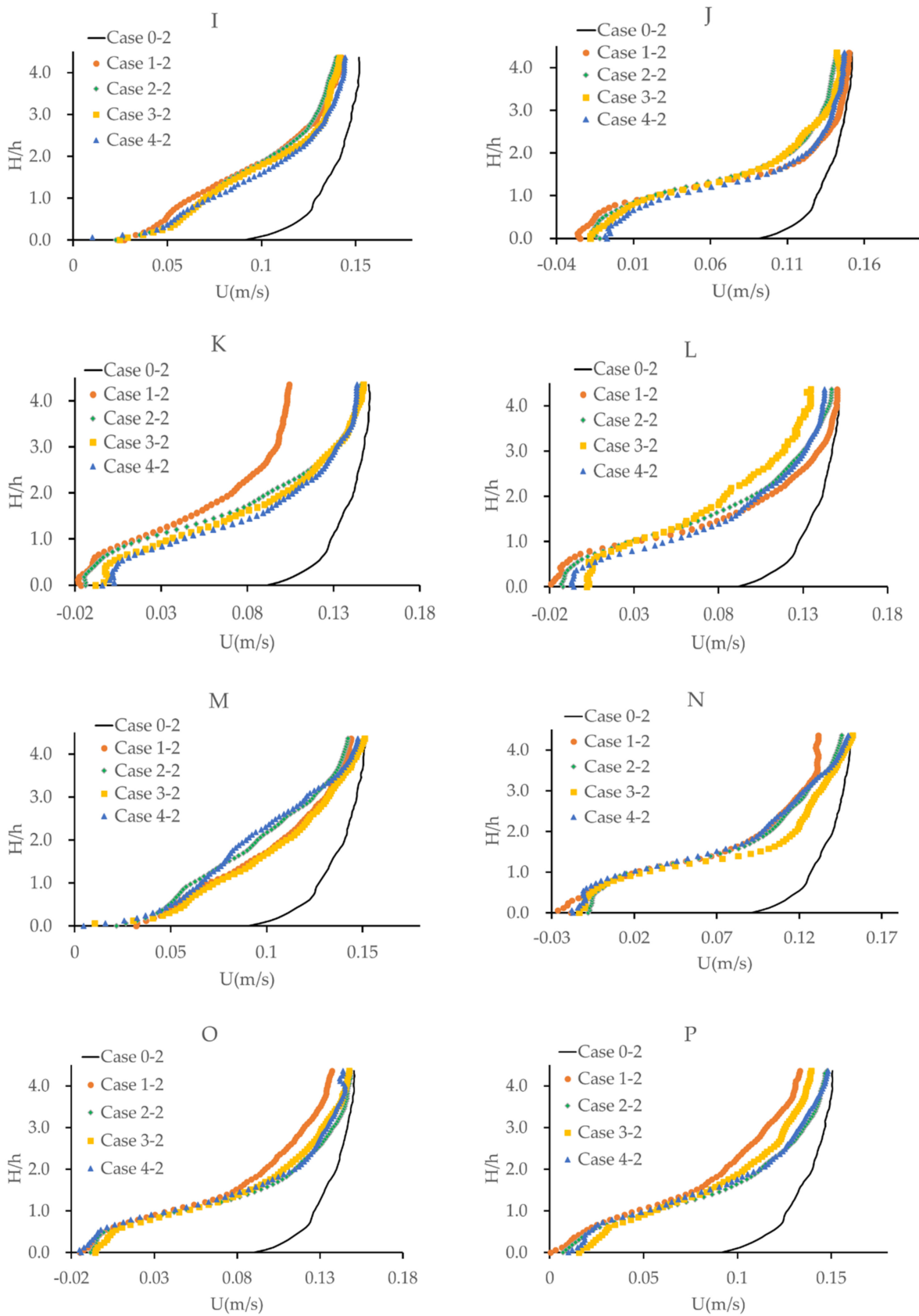
$$U = a + b \times \ln H_r \tag{1}$$

(2)   Type II & III

For the sections of Type II &III, the bottom velocity of Section C, D, J, K, L, N and O is less than 0 m/s, because these sections are in the back-vortex region where the generated vortex reverses the velocity. In this region, the longitudinal velocity distribution no longer conforms to the logarithmic distribution, but more conforms to the exponential distribution which can be fitted with Equation (2), R^2: 0.94~0.99. At this stage, the velocity increases rapidly until the dividing point and then changes to the logarithmic distribution. However, this kind of logarithmic distribution is different from Type I, and there is a certain offset in the starting coordinates of H_r which is better fitted with Equation (3), R^2: 0.83~0.99. Meanwhile, different sections have different dividing point heights. For the sections of Type II behind the reef group, the H_r of the dividing point is about 1.5, but for the sections of Type III between the two reef monocases, the H_r is about 1.2.

$$\textit{Phase I} \qquad U = a + b \times e^{cH_r} \tag{2}$$

$$\textit{Phase II} \qquad U = a + b \times \ln(H_r + c) \tag{3}$$

(3)   Type IV

For Sections G, H, I and M in the front of the reef groups, the bottom velocity of these sections is greater than 0 m/s because of the long distance from the front reefs and no effect from the back vortex. Moreover, the longitudinal velocity increases almost steadily from the bottom to the dividing point, and then increases slowly with the increase of water depth. Although there are two different acceleration modes, the longitudinal velocity distribution of all these sections can still conform to the logarithmic distribution. But similar with the Phase II of Type II &III, the logarithmic distribution of Type III has a certain offset in the starting coordinates of H_r which can be fitted with Equation (3), R^2: 0.96~0.99.

Overall, different spacing has little effect on the longitudinal velocity distribution of each section, and the distribution of the longitudinal velocity under each spacing is highly coincident. For almost all sections, the logarithmic velocity at different spacing is less than when the reefs were absent. And the longitudinal velocity of Type I & IV are two different logarithmic distributions, while the velocity distributions of Type II & III is a combination of exponential and logarithmic distributions which can be divided by a certain relative water depth H_r. Below this certain point, the longitudinal velocity no longer conforms to the logarithmic distribution and is significantly less than when the reefs were absent. Above this point, the longitudinal velocity is gradually getting close to the logarithmic distribution which is coincident with that when the reefs were absent. The specific fitting results of some representative sections can be seen in Table 2.

Table 2. Fitting results of longitudinal velocity distribution in some representative sections.

Section (Type)	u_0	Longitudinal Velocity Distribution			Section (Type)	u_0	Longitudinal Velocity Distribution			
		$U=a+b\times\ln H_r$					$U=a+b\times\ln(H_r+c)$			
		a	b	R^2			a	b	c	R^2
A (I)	0.085 m/s	0.0617	0.1042	0.98	M (IV)		0.00954	0.08163	1.23484	0.99
	0.130 m/s	0.0173	0.1051	0.98			0.11864	0.13492	2.91120	0.99
	0.170 m/s	0.0207	0.1171	0.99			0.04705	0.06567	0.59773	0.99
	0.214 m/s	0.0198	0.1013	0.98			0.23196	0.17871	4.19658	0.99

Section (Type)	u_0	Longitudinal velocity distribution							
		Phase I : $U=a+b\times e^{cH_r}$				Phase II : $U=a+b\times\ln(H_r+c)$			
		a	b	c	R^2	a	b	c	R^2
D (II)	0.085 m/s	−0.04786	0.02351	1.2781	0.99	0.11587	0.01855	−1.22938	0.90
	0.130 m/s	−0.03855	0.01055	1.91429	0.99	0.12055	0.02109	−1.19501	0.98
	0.170 m/s	−0.07181	0.04590	1.00823	0.99	0.13299	0.01851	−1.21682	0.94
	0.214 m/s	−0.02744	0.02529	1.21683	0.99	0.12385	0.01427	−1.22469	0.95
J (III)	0.085 m/s	−0.04405	0.01437	1.51288	0.99	0.13509	0.01619	−1.47371	0.99
	0.130 m/s	−0.03004	0.01074	1.56525	0.99	0.12347	0.01912	−1.45391	0.99
	0.170 m/s	−0.03531	0.01623	1.33927	0.99	0.11999	0.02513	−1.32204	0.99
	0.214 m/s	−0.02538	0.01477	1.44130	0.99	0.13196	0.01588	−1.44713	0.99

3.1.3. Vertical Velocity Distribution

Taking the flow velocity of 0.130 m/s as an example, the vertical velocity distribution of each section under different spacing are shown in Figure 7. According to the distribution pattern of vertical velocity in the vertical direction, all sections can be classified into three categories as follows:

- A, B, G, H, I and M are the front sections of the reef groups. (Type I & IV);
- D, E, F, L, O and P are the rear sections of the reef groups (Type II);
- C, J, K and N are the sections between the two reef monocases (Type III);

For Type I & IV, the vertical velocity of the section can be roughly regarded as a "V" shape distribution with the left opening. The velocity gradually increases from the bottom and reaches the maximum at the velocity dividing point which is basically 1~1.5 times the reef height. After that, the velocity decreases gradually with the increase of water depth. Among these sections, section G is greatly affected by the front and rear reef groups at the same time, the vertical velocity fluctuates on the vertical line except for the spacing of 1.25 L, but the overall change is small. This kind of section is in the upward flow affected by fish reefs, and the upwelling effect is obvious. Therefore, the vertical velocity generally increases, and the velocity at most measuring points on each section is greater than that when the reefs are absent. The comparison between different spacing conditions is obvious, which basically follows the trend: 1.25 L > 1.50 L > 0.75 L ≈ 1.00 L.

However, the vertical velocity distribution law on the sections of Type II is completely opposite to Type I & Type IV, which can be regarded as the "V" shape distribution with the right opening. The velocity decreases rapidly from the bottom and reaches the minimum value at the velocity dividing point which is basically 1~1.5 times the reef height. After that, the velocity increases gradually with the increase of water depth. Such sections are located in the back-vortex region with a large number of vortices, so the vertical velocity generally decreases and is basically less than 0 m/s. The velocity at most measuring points on each section is less than that when the reefs are absent, and there was no significant divergence between different spacing.

Besides, the vertical velocity on the section C, J, K and N of Type III can be regarded as an irregular "Z" shape distribution. When H/h < 1, the near bottom vertical velocity first decreases rapidly with the increase of water depth, and then increases rapidly with the increase of water approximately when 1 < H/h < 2.3, and finally the velocity decreases slowly with the increase of water depth. And there was also no significant difference between different spacing.
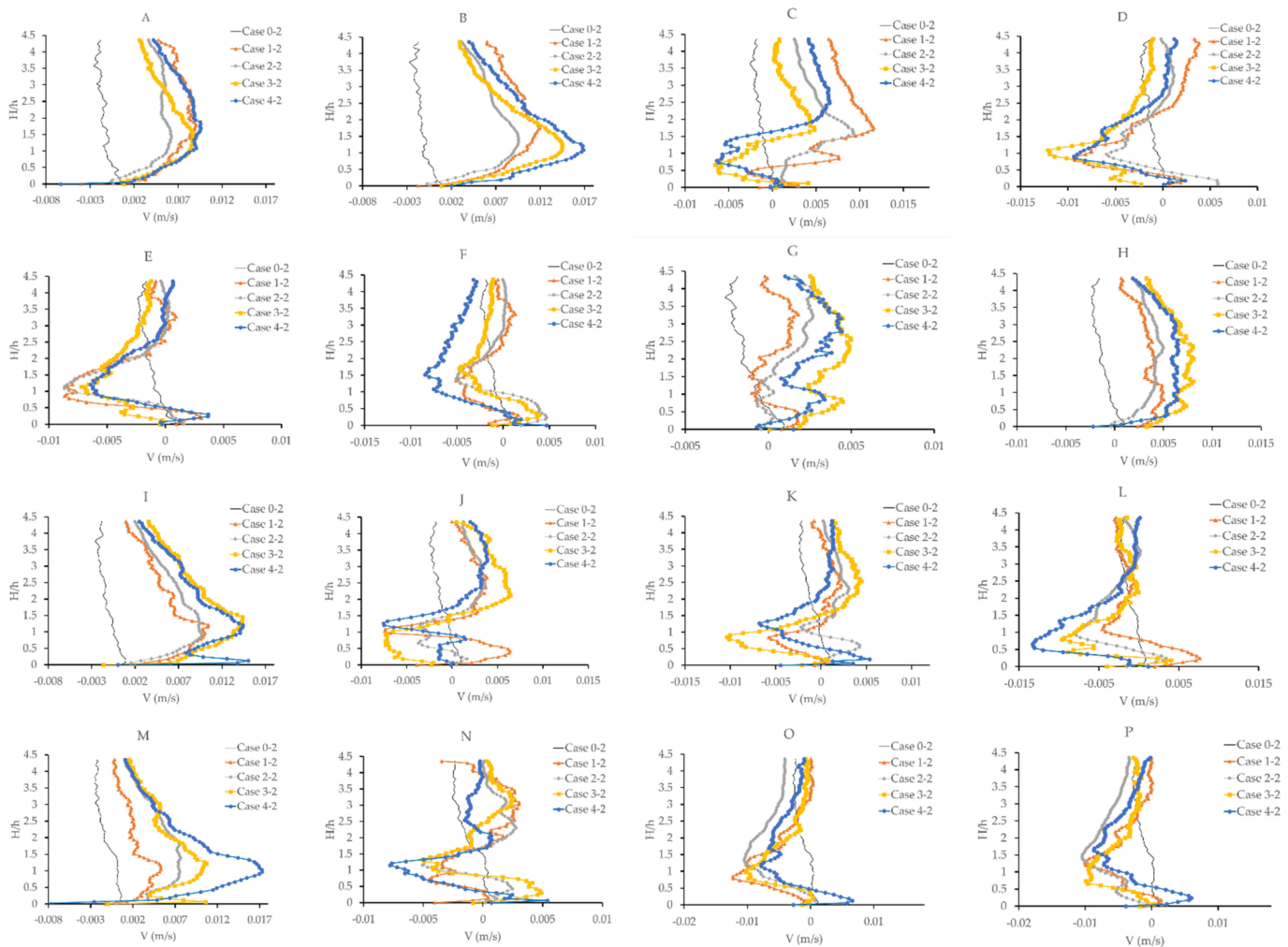

Figure 7. Vertical velocity distribution of each section of M-shaped unit reef.

3.2. Characteristics of Upwelling Flow and Back Vortex Flow Field

3.2.1. The Upwelling Flow Field

Once the artificial reef was located in the flume, the incoming flow was obstructed by the reef body, resulting in a flow separation. The upwelling observed, could promote the exchange of seawater between the upper and lower layers, increase the transport of nutrients, improve the marine primary productivity, and enhance the bait effect in the reef area, inducing a more obvious fish gathering. Therefore, the scale of the upwelling phenomenon has to be considered as an important index to evaluate the flow field effect of the artificial reefs. At present, there is no unified standard definition for the upwelling phenomenon. Based on previous research results identified in literature [57–59], this study defines as an upwelling region the area where the ratio between the vertical velocity V and the incoming velocity U is greater than or equal to 10%.

The distribution of the upwelling area induced by M-type unit reefs shows high similarities under different testing conditions, as shown in Figure 8. The upwelling area

mainly appears at the sharp corner above the first single reef upstream, and is generally fan-shaped with the sharp angle as the center. Along the direction of the flow, the scale of the rising flow area produced by the reef impact gradually decreases and at the same time, there is a small range of upwelling between the two adjacent monomeric reefs in each reef group. Figure 4 shows the upwelling region under different working conditions when the interval between reef groups in unit reef is 1.25 L.
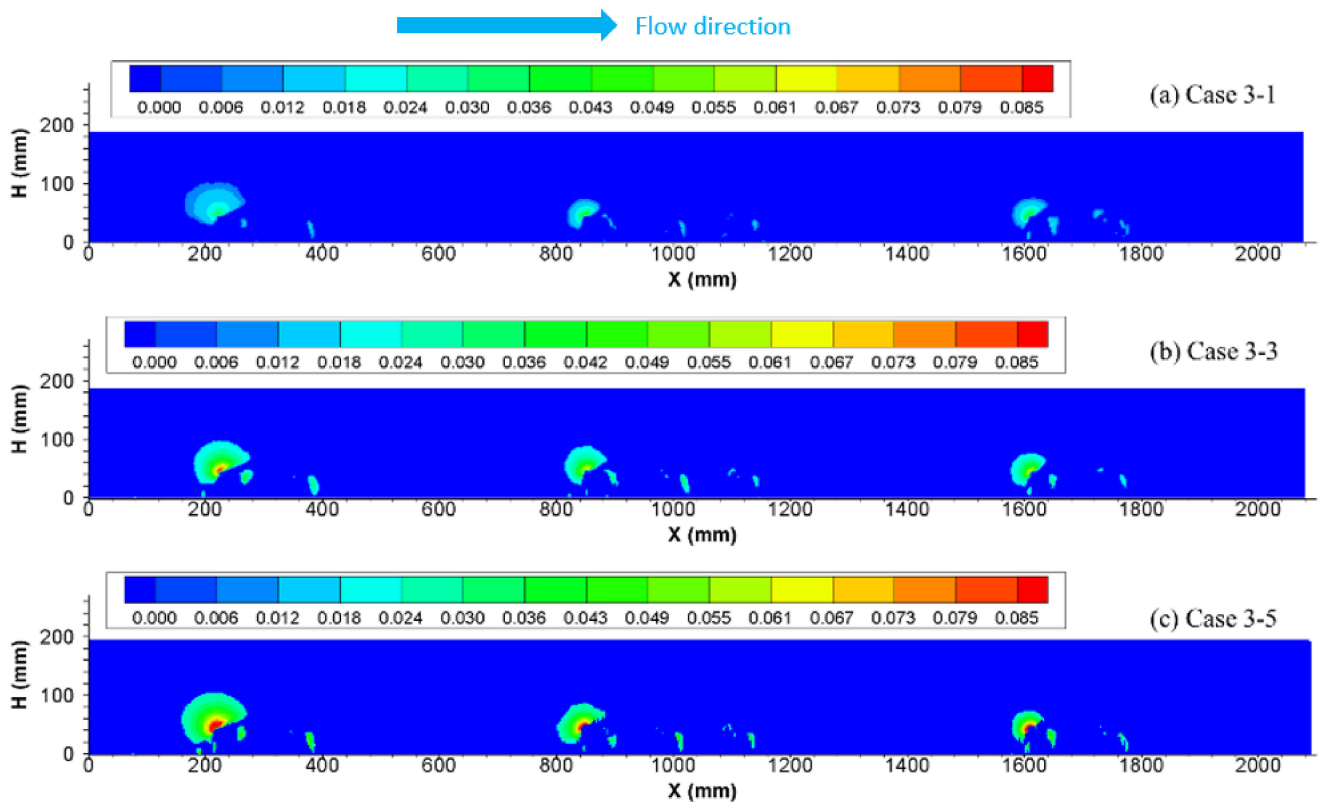

Figure 8. Upwelling area of M-shaped unit reef under different conditions. (**a**) Case 3-1; (**b**) case 3-3; (**c**) case 3-5.

The length, height and area of the upwelling region under each working condition tested within the experimental facility were considered for a comparative analysis. The maximum upwelling velocity V_{max} and the average upwelling velocity V_{ave} were used to measure the intensity of the upwelling, and the maximum upwelling height $H_{up,max}$, the maximum upwelling length $L_{up,max}$ and the total upwelling area S_{up} were used to characterize the scale of the upwelling. The height of the upwelling was calculated with the bottom of the reef as the zero point. Figure 9 shows the variation of the upwelling values for M-type reef under the different hydraulic conditions tested. Overall, the characteristic values of the upwelling seem to be increasing with the increase of the flow velocity. Analysing similar velocity conditions but different geometrical configurations, it is possible to mention that the characteristic value of the upwelling initially decreased first, then increased and then decreased again with the increase of spacing applied. The maximum value was recorded when the spacing was 1.25 L. The maximum velocity of the upwelling was about 28.78~53.56% of the incoming velocity. Relation of V for various configurations was V (1.25 L) $\approx$ V (0.75 L) > V (1.50 L) > V (1.00 L). The average velocity of the upwelling was about 13.67~16.19% of the incoming velocity, which is roughly 1.25 L > 0.75 L $\approx$ 1.50 L > 1.00 L. The maximum height of upwelling was about 1.89~2.63 times higher than that of single reef, which is roughly 1.25 L > 1.50 L > 0.75 L > 1.00 L; The maximum length of upwelling was about 1.84~2.47 times of the height of single reef, which is about 1.25 L > 0.75 L > 1.50 L > 1.00 L; The total area of upwelling was 1.25 L > 1.50 L > 0.75 L > 1.00 L.

The scale of the upwelling phenomenon generated by the first single reef of the first reef group was obviously dominant in all the upwelling areas.
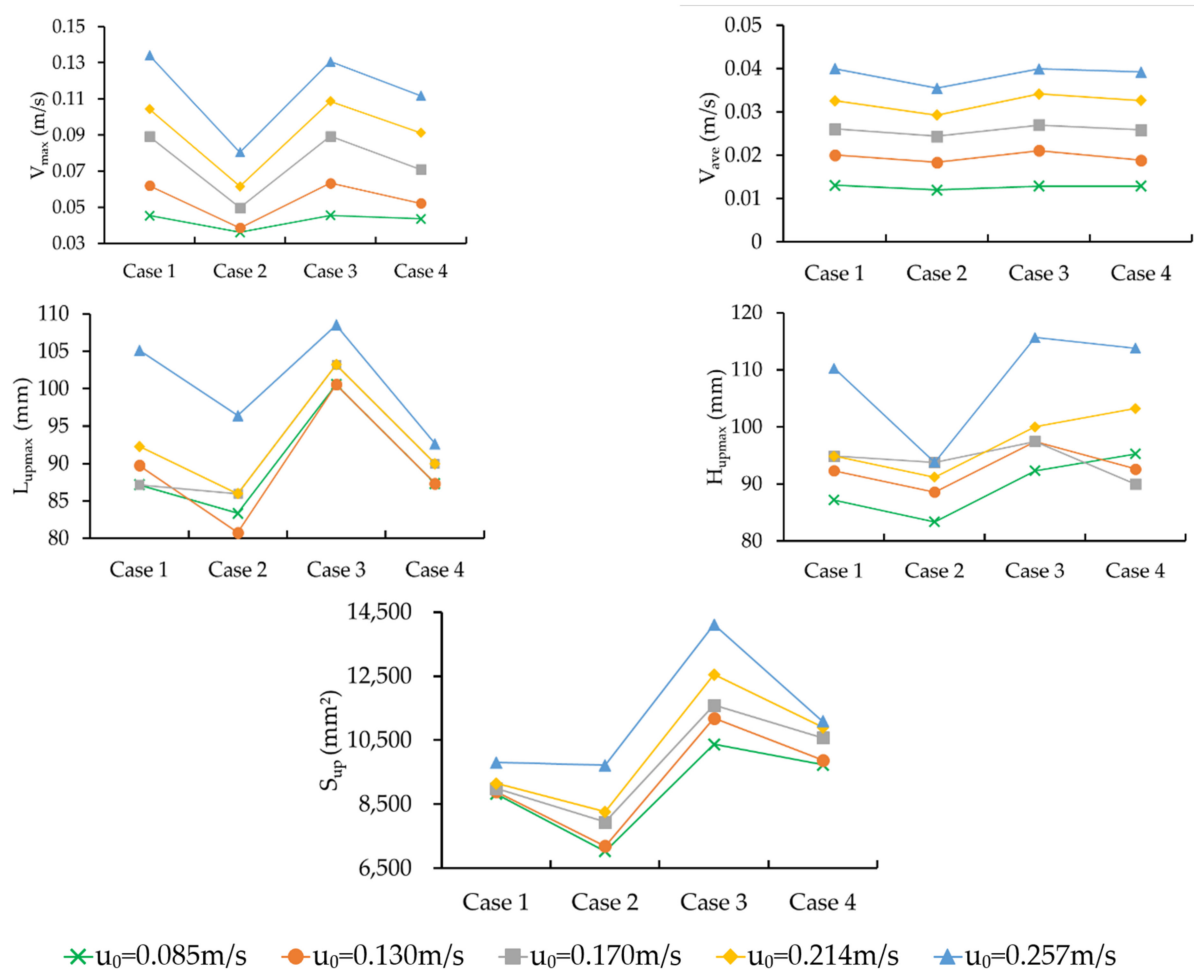

Figure 9. Upwelling values of M-shaped unit reefs under different testing conditions: V_{max}, V_{ave}, L_{upmax}, H_{upmax}, S_{up}.

3.2.2. The Back Vortex Flow Field

After the artificial reef was setup in the experimental facility, part of the incoming flow would pass through the reef and produce a low turbulence area on its back. Because there are a lot of vortices generated in this region, this was called back vortex area. The eddy current structure in this area was generally stable, which can support the fact that these conditions facilitate the deposition of nutrients, and provide a place for fish and other organisms to inhabit, avoid enemies and feed. The scale of the back vortex is also an important index to evaluate the effect on the flow field induced by artificial reefs. In this study, the back vortex region was defined as a slow flow region where vortices formed on the back or inside of a single reef.

The maximum height H_{bmax}, the maximum length L_{bmax} and the total area S_b of the back vortex were used to characterize the scale and magnitude of the back vortex and were quantified by looking at the experiments and analysing the flow field generated. The height of the back vortex was calculated with the bottom of the reef as the zero point. The characteristic values of the back vortex under each working condition are compared and analyzed and displayed in Figure 10.
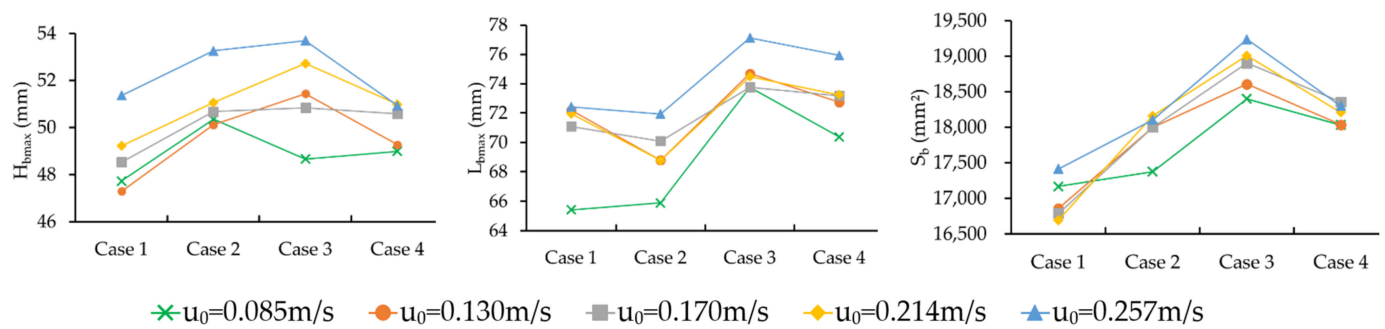
Figure 10. Characteristic values of the back vortex region recorded for M-shaped unit reefs under different configurations: H_{bmax}, L_{bmax}, S_b.

Under different conditions, the distribution of the back vortex region showed a high degree of similarity too. The back vortex region mainly appeared between every two adjacent reefs in each reef group and at the back of the last reef in each configuration. In general, seven large back vortex regions were spotted in the whole flow field, with one or two clockwise large vortices in each region. Furthermore, there were also small eddy currents in the reef, but the scale was too small hence could be ignored. Along the flow direction, there was no obvious rule characterizing the magnitude and scale of each back vortex area, and the difference between them was small, however the scale on the back of the first single reef was usually recorded as the largest.

Figure 10 shows the variation of the characteristic values of the back vortices within M-type reefs under different configurations. Similarly to the variation of the upwelling characteristic values, those of the back vortex increased with the increase of the velocity. However, at the same velocity, the characteristic values of the back vortex had obvious differences, but no uniform variation law was identified. The maximum height of the back vortex was about 1.07~1.22 times of the height of the single reef, and the total area of the back vortex firstly increased and then decreased with the increase of the spacing, reaching the maximum value when the spacing was 1.25 L > 1.50 L > 1.00 L > 0.75 L. The maximum length of the back vortex firstly decreased, then increased and then decreased with the increase of the spacing, (1.25 L > 1.50 L > 0.75 L > 1.00 L), which is about 1.49~1.75 times of the height of the single reef.

3.3. Evaluation of Each Configuration Tested Based on Impacts of the Hydrodynamics

The artificial reefs have enormous ecological and environmental effects. The upwelling generated by the obstruction of the reef can enable the transportation of nutrients in the upper and lower layers of sweater, and at the same time the back vortex generated on the back of the reef provide a place for fish to rest, avoid natural enemies and find food. Therefore, reef groups improve the condition of current flow fields within the marine environment which cause an increasing production of marine biological resources. In order to better judge the effects of the M-Type reefs on the flow field to figure out which layout spacing is the one creating the most favorable conditions to the marine environment, in this paper 11 hydrodynamic indexes and 1 extra economic index were selected for evaluation. Between these indexes there are velocity distribution, the upwelling and the back vortex, the turbulence intensity and the economic cost and their effects are combined to provide a final evaluation score associated with each spacing layout tested under each configuration. Finally, the comprehensive score of each spacing is calculated by adopting a weighting method, and the best scheme obtained and presented was the one with the largest value calculated.

3.3.1. Entropy Method

Entropy was introduced firstly within thermodynamics [57], and then it was developed as a theory to quantify the degree of uncertainty within a system [58–61]. The basic

idea of the entropy method is to reflect the degree of differentiation of evaluation objects from the perspective of the index entropy. The smaller is the entropy value of an index, the more useful information it provides and greater is the corresponding weight. On the contrary, the higher is the entropy, the less useful information the index provides, and the less important the index is.

The entropy method is an objective weighting method, which can overcome human subjective factors and objectively reflect the utility value of each index. Since it was proposed, it has been widely used in the evaluation of problems in many fields, as well as the optimization of multi working conditions and different schemes [62–69]. There is no limit on the number of indexes to be selected, and it has strong practicability and wide application range. The specific steps of the entropy method can be listed as follows:

(1) Raw data standardization:

$$Positive\ index \cdots \cdots x'_{ij} = \frac{x_{ij} - \min\{x_{1j}, \cdots, x_{nj}}{\max\{x_{1j}, \cdots, x_{nj} - \min\{x_{ij}, \cdots, x_{nj}}} \tag{4}$$

$$Negative\ index \cdots x'_{ij} = \frac{\max\{x_{1j}, \cdots, x_{nj} - x_{ij}}{\max\{x_{1j}, \cdots, x_{nj} - \min\{x_{ij}, \cdots, x_{nj}}} \tag{5}$$

Among all the indexes, only the economic cost index can be negative. Because the logarithm is used in the entropy method, the normalized value cannot be used directly. In order to solve the influence of the negative number, the standardized value is transformed as follows:

$$Z_{ij} = x'_{ij} + A \tag{6}$$

where x_{ij} is the original value of the *i*-th sample and j index, x_{ij}' is the standardized index value, Z_{ij} is the value after translation, and *A* is the translation amplitude.

(2) Calculation of the characteristic proportion or contribution (p_{ij}) of the *i*-th evaluation object under the *j*-th index:

$$p_{ij} = \frac{Z_{ij}}{\sum\limits_{i=1}^{n} Z_{ij}} \quad (i = 1, 2 \ldots, n; j = 1, 2 \ldots, m) \tag{7}$$

where *n* is the number of samples (spacing, *n* = 4 in this paper) and *m* is the number of indicators.

(3) Calculation of the entropy value (e_j) of index *j*:

$$e_j = -k \sum_{i=1}^{n} p_{ij} \ln(p_{ij}) \tag{8}$$

where, $k = \frac{1}{\ln n}, e_j \geq 0$.

(4) Calculation of the difference coefficient (g_j) of index *j*:

$$g_j = 1 - e_j \tag{9}$$

(5) Normalization of the difference coefficient and calculation of the weight of index *j* (W_j):

$$W_j = \frac{g_j}{\sum\limits_{i=1}^{m} g_j} \quad (j = 1, 2 \ldots \ldots m) \tag{10}$$

(6)   Calculation of the comprehensive score (Y_i) of each index of the *i*-th evaluation object:

$$Y_i = \sum_{i=1}^{m} W_j p_{ij} \qquad (11)$$

3.3.2. Weight Optimization

In order to explore the balance between ecological benefit and economic cost for the application of artificial reefs, two evaluation indexes were established. The first one was the hydrodynamic index, and the second one incorporated the contribution of both hydrodynamic and economic cost indexes. For the economic cost index, through a preliminary field investigation and literature research, it was found the cost of each empty volume occupied by the single square ecological reef (Table 3). However, it was decided that if the cost of each empty volume was directly taken as the economic cost index, the value of the index was equal under all the design spacing, and this index would not play a role in the comprehensive evaluation. Therefore, in order to improve the rationality of the evaluation index, this study puts forward the cost index per square meter of unit reef through the total cost of unit reef and its area (the total cost is the construction price of the reef, and the cost per square meter is calculated based on the cost of the reef and the area of the reef group), and takes it as the economic cost index. The specific results are shown in Table 3.

Table 3. Economic cost evaluation index of flow field effect of M-shaped unit reef.

Spacing	Length of the Experimental Section (mm)	Width of the Experimental Section (mm)	Representative Area (m²)	Cost per Square Meter of the Monocase (CNY)	Cost of the Experimental Section (CNY)	Cost per Square Meter (CNY/m²)
0.75 L	1400	800	2800	435.07	88,319.21	31.5426
1.00 L	1600	800	3200	435.07	88,319.21	27.5998
1.25 L	1800	800	3600	435.07	88,319.21	24.5331
1.50 L	2000	800	4000	435.07	88,319.21	22.0798

According to the entropy method Equations (4)–(11), the weight of each evaluation index under the five flow rates tested was calculated. In order to make the weight more reasonable, the arithmetic mean value of the weight of each index under the five flow rates was selected as the final weight, as shown in Table 4. It can be seen from the table that the top three index weights are maximum length of upwelling (10.71%), average vertical turbulence intensity (9.74%) and average longitudinal turbulence intensity (9.73%), respectively. The weight of upwelling index was 40.77%, ranking first, among which the weight of the maximum length and total area of upwelling was larger. The weight of the back vortex index was 23.89%, ranking second, and the weight of the maximum length of the back vortex was the largest. The weight of turbulence intensity index was 19.47%, ranking third, and the weight of longitudinal and vertical indexes was equal. Finally, the weight of the economic cost index was 7.19%.

Table 4. Weight system for each variable affecting the flow field around M-shaped unit reefs.

Index Type	No Economic Cost Index	Including Economic Cost Index	Index	No Economic Cost Index	Including Economic Cost Index
	Weight I	Weight II		Weight I	Weight II
Velocity distribution	9.35%	8.68%	U_{ave}	9.35%	8.68%
Upwelling	43.94%	40.77%	v_{max}	6.97%	6.47%
			v_{ave}	7.44%	6.90%
			H_{upmax}	7.92%	7.35%
			L_{upmax}	11.55%	10.71%
			S_{up}	10.06%	9.34%
Back vortex	25.73%	23.89%	H_{bmax}	8.13%	7.55%
			L_{bmax}	9.65%	8.96%
			S_b	7.95%	7.38%
Turbulence intensity	20.98%	19.47%	Mean longitudinal turbulence intensity	10.48%	9.73%
			Mean vertical turbulence intensity	10.50%	9.74%
Economic cost	-	7.19%	Cost per square meter	-	7.19%

Note: U_{ave}; The fitting results of representative sections C and J between the two reef monocases and behind the reef groups were selected to calculate the average longitudinal velocity. Turbulence intensity: the calculation results of this variable are from published papers [20].

3.3.3. Analysis of Evaluation Results

According to the determined index weight system, the scores of each spacing under five design flow rates were calculated according to Equation (8). In order to compare and analyze the results associated with different spacing, the arithmetic average of the five flow rates was used as the comprehensive score y of each interval, and the comprehensive scores of the two index systems were recorded as Y_1 and Y_2 respectively.

Figure 11 shows the final comprehensive score Y for the four intervals. When considering the hydrodynamic index, the comprehensive scores followed the trend Y (1.25 L) > Y (1.50 L) > Y (0.75 L) > Y (1.00 L), with the gap between 1.50 L and 0.75 L which was very small. The comprehensive score of the scenario 1.25 L was significantly higher than any other spacing, being 1.871, 2.117 and 4.747 times of 1.50 L, 0.75 L and 1.00 L, respectively. The results showed that when the spacing between each reef group in a unit reef was 1.25 times of the original design interval, the flow field effect had the maximum impact, and the scores of up-flow, back eddy current and turbulence intensity were all reaching maximum values for all the four kinds of spacing. It can also be found that when the distance between the reefs increased, the comprehensive score decreased significantly.

This outcome indicated that the critical value of the scale of the M-type reef unit reefs had been reached after 1.25 times of the original design distance, and it was not suitable to increase the spacing anymore. The original design spacing was the worst among the four spaces tested, with score less than 0.1, only 31.5% of the average comprehensive score of the other three spacing setups. It showed that the scale of the original design spacing was not suitable for M-type unit reefs, and the cooperative effect between the reefs couldn't be fully exerted under this spacing.
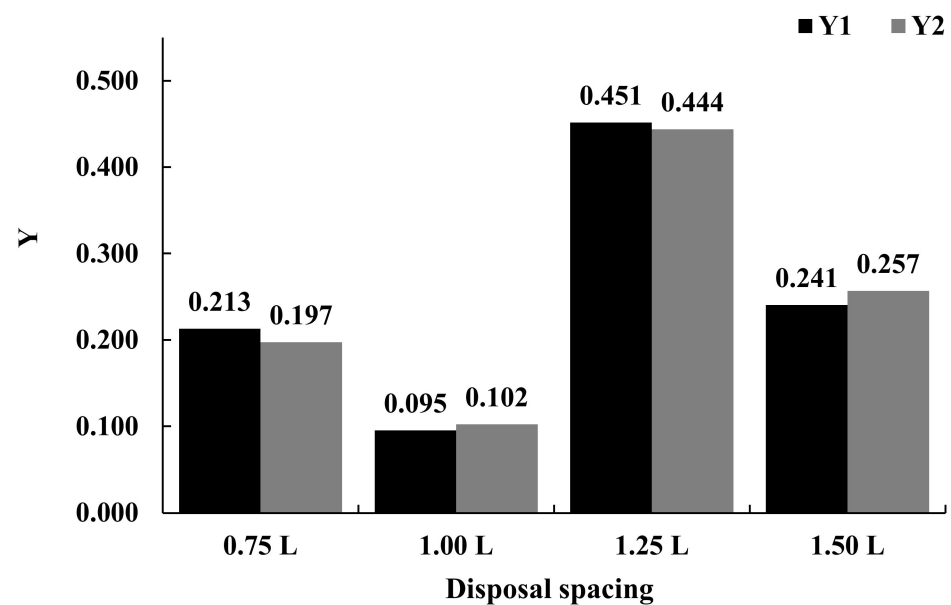
Figure 11. Comprehensive evaluation score of flow field effect of M-shaped unit reef.

The results of the evaluation taking in consideration the cost index are consistent with those focusing on the hydrodynamic characteristics. The comprehensive scores followed this trend: 1.25 L > 1.50 L > 0.75 L > 1.00 L, the score of scenario 1.25 L was 2.254 and 4.353 times of 0.75 L and 1.00 L, respectively. After the cost index was included, the score of 0.75 L and 1.25 L had decreased, and the scores of 1.00 L and 1.50 L had risen, but the change range was not enough to affect the final evaluation results. This confirmed that the economic cost has negligible influence on the M-type unit reefs application of different sizes and spacing. Overall, the cost per square meter of the unit reef only accounts for less than 8%. In fact, the flow field effect and ecological benefit of the artificial reefs are considered when deciding quantities of M-type artificial reef to implement. In conclusion, from the theoretical and practical point of view, it is suggested that the size of M-type reef unit reef should be adjusted when the reef is cast, and the interval between reef groups should be changed to 1.25 times of the original interval.

3.3.4. Analysis on the Application of the Adjusted Layout Scheme

According to the evaluation results for the system that only considers the hydrodynamic characteristics and the economic cost, and comprehensively considers the ecological benefits and economic cost, it is suggested that the unit reef spacing of M-type reef should be expanded by 25% on the basis of the original spacing. In addition, through comparative analysis, it is found that the differences of upwelling, back vortex and other hydrodynamic characteristics between reef groups composed of 6 individual reefs and 4 individual reefs are negligible. Therefore, it is suggested that at the actual site all reef groups should be composed of 4 individual reefs to further reduce economic input. For this configuration, the interval between unit reef groups was 23.57 m, and the side length of square unit reef was 52.5 m (Figure 12). The M-type reef unit reef group was composed of five unit reefs with a spacing of 100 m. The schematic diagram before and after adjustment is shown in Figure 13. It can be seen from Table 5 that the flow field effect of unit reef and unit reef group after spatial layout adjustment is enhanced compared with the original spacing, the number and cost of single reef are reduced by 10%, and the affected flow field area is increased by 10% and 5% respectively, which can obtain greater ecological benefits with less economic input and create a better living environment for more marine organisms.
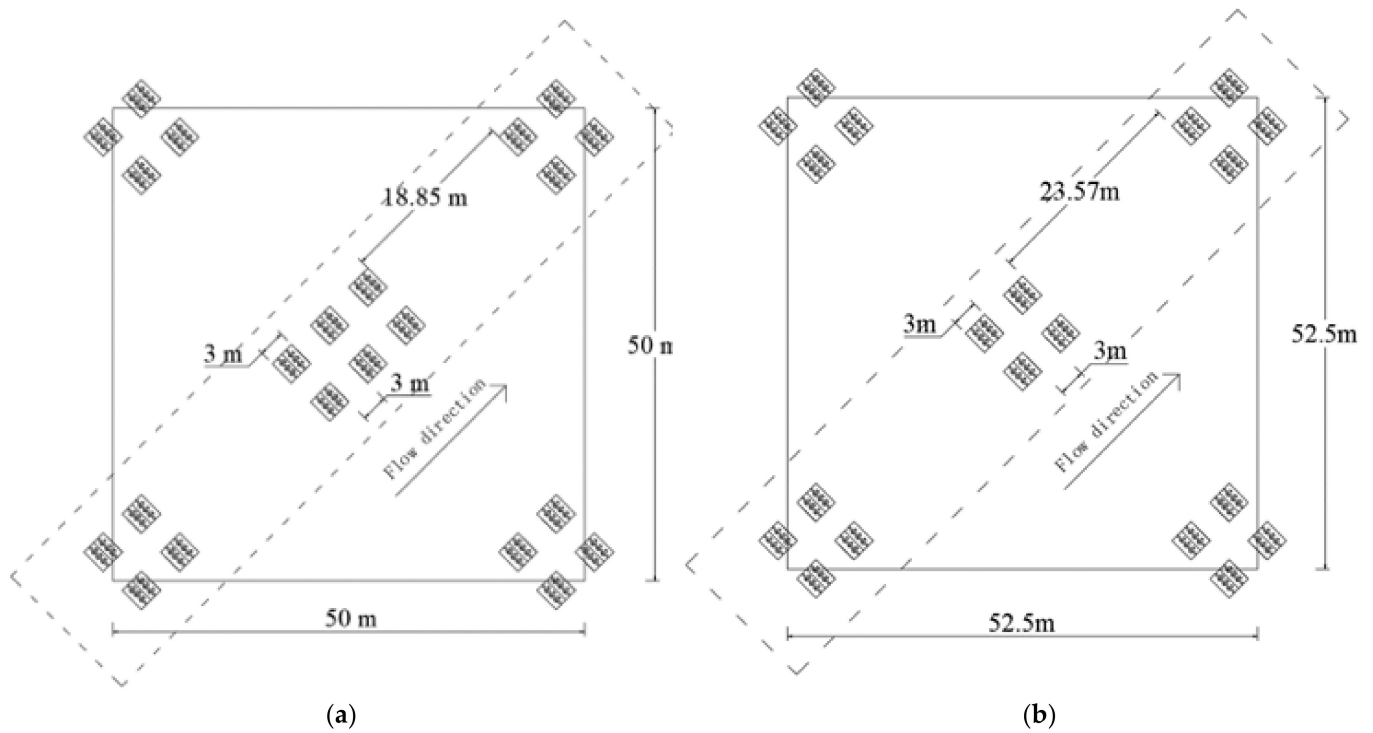
Figure 12. Comparison of M-shaped unit reef before and after the adjustment. (**a**) Original design spacing; (**b**) adjusted spacing.
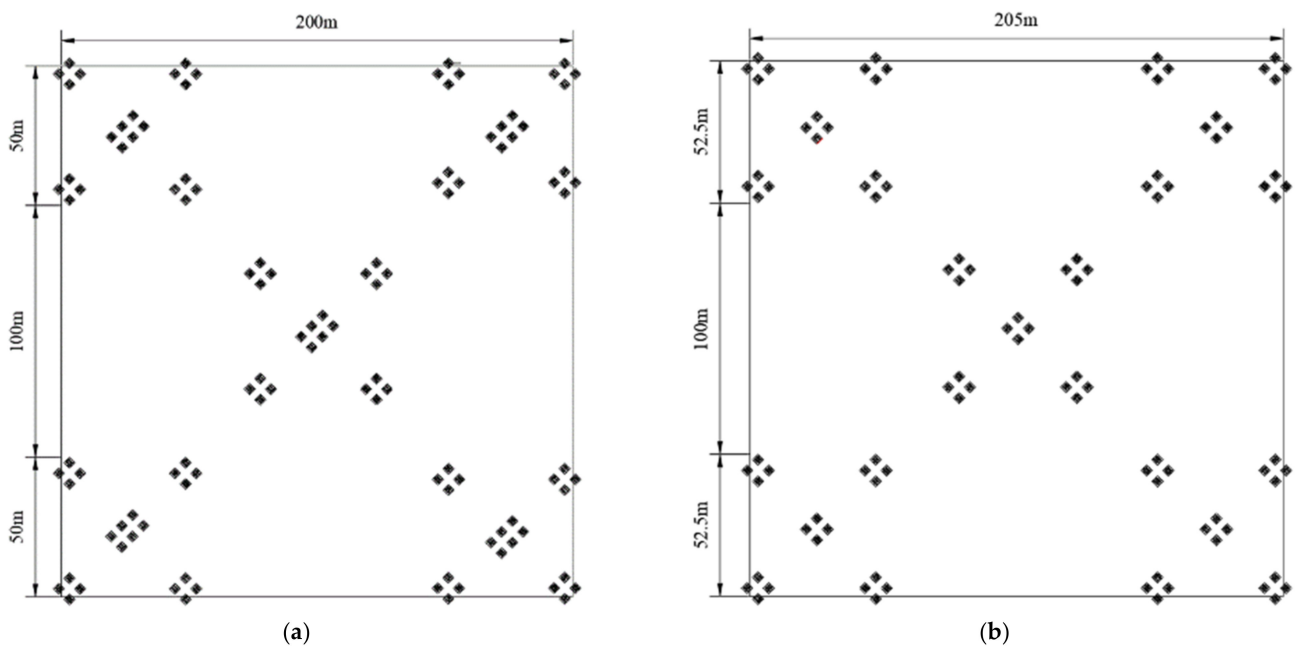

Figure 13. Comparison of M-shaped reef cluster before and after the adjustment. (**a**) Original design spacing; (**b**) adjusted spacing.

Table 5. Comparison of M-shaped reef layout before and after adjustment.

	Side Length (m)	Area (m^2)	Number of Monocases	Economic Cost (Yuan)
Original design unit reef	50	2500	22	9571.54
Adjusted unit reef	52.5	2756.25	20	8701.40
Original design reef cluster	200	40,000	110	47,857.70
Adjusted reef cluster	205	42,025	100	43,507.00

4. Conclusions

Nowadays, artificial reefs are increasingly being adopted because to date they have demonstrated to provide shelter, food and other necessary elements for biodiversity and a productive ocean [70–72]. As a consequence to these benefits, marine life becomes rich, attracting divers and anglers and therefore it could also enhance the tourism and commercial fishing of many local areas around the world improving their economies.

In this paper, M-Type artificial reefs are investigated to determine the benefits of their presence on the hydrodynamics, and more in particular on the upwelling and back vortex characteristics they induced on the flow field. Effects have been analyzed via conducting a series of experimental tests within a flume and the entropy method was implemented to conduct a comprehensive evaluation based on different evaluation systems. The main conclusions can be summarized as follows:

(1) According to the longitudinal velocity distribution of all sections, it was found that the longitudinal velocity distribution of the sections in front of the reef groups (Type I & IV) conforms to logarithmic distributions which can be fitted with Equations (1) and (3) respectively. While the longitudinal velocity distribution of sections between the two reef monocases and behind the reef groups (Type II & III) is a combination of exponential and logarithmic distributions which fitted with Equations (2) and (3), and there is a little difference between the dividing point height of Type II and III.

(2) By comparing the flow field under different hydraulic conditions and configurations, the experimental results show that, in general, the eigenvalues of both upwelling and back vortex increase with the increase of the velocity when the spacing is kept uniform. For similar velocity, the maximum values of both upwelling and back vortex are obtained when the distance between unit reefs is 1.25 L.

(3) Based on the hydrodynamic characteristics and the economic cost, the entropy method was used to evaluate the flow field effect induced by M-shaped reef under four spacing setups. The comprehensive score obtained from large to small was Y (1.25 L) > Y (1.50 L) > Y (0.75 L) > Y (1.00 L). The ecological benefits and the economic cost were considered, and it is suggested that the original design spacing should be increased by 25% when the square ecological unit reef is put into practice. This suggestion can be considered as a reference for the construction of M-Type artificial reef in coastal areas.

(4) Through comparative analysis, it is suggested that the M-type reef groups should be further changed into four individual reefs. In fact, after this adjustment was made, the cost of the unit reef was reduced by 10%, while the influence range on the flow field increased by 10%. Therefore, greater ecological benefits could be obtained with less economic input.

To the author's knowledge, no other studies are available in literature with M-Type artificial reefs, therefore it was not possible to compare these results with those that have been obtained with dissimilar artificial reefs and with different flow conditions and flume dimensions. Due too many variables in place, it is impossible to compare too unrelated features, therefore this manuscript focused on explaining the results obtained rather than generating a broad and vague discussion not applicable in this case. Within this study, the artificial reef was fixed on the sea bed, as it should be within the real scenario, and particular focus was directed on investigating the hydraulic features generated, however, the stability of the artificial structure should be investigated. Further research will also focus on the interaction of similar configurations with unsteady flow conditions and a variety of wave profiles characterized by dissimilar amplitudes and frequencies, representing features that may be typical of climate change [73,74].

References

1. Laxe, F.G.; Bermúdez, F.M.; Palmero, F.M.; Novo-Corti, I. Governance of the fishery industry: A new global context. *Ocean Coast. Manag.* **2018**, *153*, 33–45. [CrossRef]
2. Halpern, B.S.; Frazier, M.; Potapenko, J.; Casey, K.S.; Koenig, K.; Longo, C.; Lowndes, J.S.; Rockwood, R.C.; Selig, E.R.; Selkoe, K.A.; et al. Spatial and temporal changes in cumulative human impacts on the world's ocean. *Nat. Commun.* **2015**, *6*, 7615. [CrossRef]
3. Nilsson, J.A.; Fulton, E.A.; Johnson, C.R.; Haward, M. How to Sustain Fisheries: Expert Knowledge from 34 Nations. *Water* **2019**, *11*, 213. [CrossRef]
4. Watson, R.A.; Tidd, A. Mapping nearly a century and a half of global marine fishing: 1869–2015. *Mar. Policy* **2018**, *93*, 171–177. [CrossRef]
5. Svane, I.; Petersen, J.K. On the problems of epibioses, fouling and artificial reefs, a review. *Mar. Ecol. Pubbl. Stn. Zool. Napoli* **2001**, *22*, 169–188. [CrossRef]
6. Lima, J.S.; Zalmon, I.R.; Love, M. Overview and trends of ecological and socioeconomic research on artificial reefs. *Mar. Environ. Res.* **2019**, *145*, 81–96. [CrossRef] [PubMed]
7. Otake, S. Design and Creation of Fishing Grounds in Japan with Artificial Reefs. In *Modern Fisheries Engineering*, 1st ed.; CRC Press: Boca Raton, FL, USA, 2020; ISBN 9780429328039.
8. Manajit, N.; Yasook, N.; Putsa, S.; Tiaye, R.; Amornpiyakrit, T.; Chanrachkij, I.; Sulit, V.T. Benchmarking the adoption of fish enhancing devices in Southeast Asian waters: The coastal waters of Thailand in focus. *Fish People* **2019**, *17*, 12–17.
9. Wang, G.; Wan, R.; Wang, X.X.; Zhao, F.F.; Lan, X.Z.; Cheng, H.; Theng, W.Y.; Guan, Q.L. Study on the influence of cut-opening ratio, cut-opening shape, and cut-opening number on the flow field of a cubic artificial reef. *Ocean Eng.* **2018**, *162*, 341–352. [CrossRef]
10. Haro, A.; Castro-Santos, T.; Noreika, J.; Odeh, M. Swimming performance of upstream migrant fishes in open-channel flow: A new approach to predicting passage through velocity barriers. *Can. J. Fish. Aquat. Sci.* **2004**, *61*, 1590–1601. [CrossRef]
11. Yoon, H.-S.; Kim, D.; Na, W.-B. Estimation of effective usable and burial volumes of artificial reefs and the prediction of cost-effective management. *Ocean Coast. Manag.* **2016**, *120*, 135–147. [CrossRef]
12. Falcao, M.; Santos, M.N.; Vicente, M.; Monteiro, C.C. Biogeochemical processes and nutrient cycling within an artificial reef off Southern Portugal. *Mar. Environ. Res.* **2007**, *63*, 429–444. [CrossRef]
13. Reeds, K.A.; Smith, J.A.; Suthers, I.M.; Johnston, E.L. An ecological halo surrounding a large offshore artificial reef: Sediments, infauna, and fish foraging. *Mar. Environ. Res.* **2018**, *141*, 30–38. [CrossRef]
14. Zhang, J.; Zhu, L.; Liang, Z.; Sun, L.; Nie, Z.; Wang, J.; Xie, W.; Jiang, Z. Numerical Study of Efficiency Indices to Evaluate the Effect of Layout Mode of Artificial Reef Unit on Flow Field. *J. Mar. Sci. Eng.* **2021**, *9*, 770. [CrossRef]
15. Rinkevich, B. The Active Reef Restoration Toolbox is a Vehicle for Coral Resilience and Adaptation in a Changing World. *J. Mar. Sci. Eng.* **2019**, *7*, 201. [CrossRef]
16. Bruneel, S.; Van Echelpoel, W.; Ho, L.; Raat, H.; Schoeters, A.; De Troyer, N.; Sor, R.; Ponton-Cevallos, J.; Vandeputte, R.; Van der heyden, C.; et al. Assessing the Drivers behind the Structure and Diversity of Fish Assemblages Associated with Rocky Shores in the Galapagos Archipelago. *J. Mar. Sci. Eng.* **2021**, *9*, 375. [CrossRef]
17. Zhu, H.; Liu, X.; Cheng, S.; Wang, J. Effects of Artificial Reefs on Phytoplankton Community Structure in Baiyangdian Lake, China. *Water* **2021**, *13*, 1802. [CrossRef]
18. Collins, K.J.; Jensen, A.C.; Lockwood, A.P.M. Fishery Enhancement Reef Building Exercise. *Chem. Ecol.* **1990**, *4*, 179–187. [CrossRef]
19. Godoy, E.A.S.; Almeida, T.C.M.; Zalmon, I.R. Fish assemblages and environmental variables on an artificial reef north of Rio de Janeiro, Brazil. *ICES J. Mar. Sci.* **2002**, *59*, S138–S143. [CrossRef]
20. Shu, A.; Qin, J.; Rubinato, M.; Sun, T.; Wang, M.; Wang, S.; Wang, L.; Zhu, J.; Zhu, F. An Experimental Investigation of Turbulence Features Induced by Typical Artificial M-Shaped Unit Reefs. *Appl. Sci.* **2021**, *11*, 1393. [CrossRef]
21. Androulakis, D.N.; Dounas, C.G.; Banks, A.C.; Magoulas, A.N.; Margaris, D.P. An Assessment of Computational Fluid Dynamics as a Tool to Aid the Design of the HCMR-Artificial-ReefsTM Diving Oasis in the Underwater Biotechnological Park of Crete. *Sustainability* **2020**, *12*, 4847. [CrossRef]

22. Glarou, M.; Zrust, M.; Svendsen, J.C. Using Artificial-Reef Knowledge to Enhance the Ecological Function of Offshore Wind Turbine Foundations: Implications for Fish Abundance and Diversity. *J. Mar. Sci. Eng.* **2020**, *8*, 332. [CrossRef]

23. Chie, L.H.; Abd Wahab, A.K. Derivation of Engineering Design Criteria for Flow Field Around Intake Structure: A Numerical Simulation Study. *J. Mar. Sci. Eng.* **2020**, *8*, 827. [CrossRef]

24. Wu, S.; Rubinato, M.; Gui, Q. SPH Simulation of Interior and Exterior Flow Field Characteristics of Porous Media. *Water* **2020**, *12*, 918. [CrossRef]

25. Li, C.-Y.; Shih, R.-S.; Weng, W.-K. Visualization Investigation of Energy Dissipation Induced by Eddy Currents for a Solitary-Like Wave Passing over Submerged Breakwater Sets. *J. Mar. Sci. Eng.* **2020**, *8*, 834. [CrossRef]

26. Ma, Y.; Kuang, C.; Han, X.; Niu, H.; Zheng, Y.; Shen, C. Experimental Study on the Influence of an Artificial Reef on Cross-Shore Morphodynamic Processes of a Wave-Dominated Beach. *Water* **2020**, *12*, 2947. [CrossRef]

27. Ozalp, M.K.; Miller, L.A.; Dombrowski, T.; Braye, M.; Dix, T.; Pongracz, L.; Howell, R.; Klotsa, D.; Pasour, V.; Strickland, C. Experiments and Agent Based Models of Zooplankton Movement within Complex Flow Environments. *Biomimetics* **2020**, *5*, 2. [CrossRef] [PubMed]

28. Rubinato, M.; Heyworth, J.; Hart, J. Protecting Coastlines from Flooding in a Changing Climate: A Preliminary Experimental Study to Investigate a Sustainable Approach. *Water* **2020**, *12*, 2471. [CrossRef]

29. Harris, L.; Liang, D.; Shao, S.; Zhang, T.; Roberts, G. MPM simulation of solitary wave run-up on permeable boundaries. *Appl. Ocean. Res.* **2021**, *111*, 102602. [CrossRef]

30. Kazemi, E.; Koll, K.; Tait, S.; Shao, S. SPH modelling of turbulent open channel flow over and within natural gravel beds with rough interfacial boundaries. *Adv. Water Resour.* **2020**, *140*, 103557. [CrossRef]

31. Kazemi, E.; Tait, S.; Shao, S. SPH-based numerical treatment of the interfacial interaction of flow with porous media International. *J. Numer. Methods Fluids* **2020**, *92*, 219–245. [CrossRef]

32. Jiang, Z.; Liang, Z.; Zhu, L.; Guo, Z.; Tang, Y. Effect of hole diameter of rotary-shaped artificial reef on flow field. *Ocean. Eng.* **2020**, *197*, 106917. [CrossRef]

33. Cardenas-Rojas, D.; Mendoza, E.; Escudero, M.; Verduzco-Zapata, M. Assessment of the Performance of an Artificial Reef Made of Modular Elements through Small Scale Experiments. *J. Mar. Sci. Eng.* **2021**, *9*, 130. [CrossRef]

34. Jiang, Z.; Zhu, L.; Mei, J.; Guo, Z.; Cong, W.; Liang, Z. Preliminary study on the boundary layer of an artificial reef with regular grooves surface structure. *Ocean. Eng.* **2021**, *219*, 108355. [CrossRef]

35. Zheng, Y.; Kuang, C.; Gu, J.; Han, X.; Ma, Y. Experimental Investigation on Flow Patterns Induced by a Twin-Block Perforated Artificial Reef. In Proceedings of the 30th International Ocean and Polar Engineering Conference, Shanghai, China, 11–16 October 2020.

36. Wang, X.; Liu, X.; Tang, Y.; Zhao, F.; Luo, Y. Numerical Analysis of the Flow Effect of the Menger-Type Artificial Reefs with Different Void Space Complexity Indices. *Symmetry* **2021**, *13*, 1040. [CrossRef]

37. Kuang, C.; Ma, Y.; Han, X.; Pan, S.; Zhu, L. Experimental Observation on Beach Evolution Process with Presence of Artificial Submerged Sand Bar and Reef. *J. Mar. Sci. Eng.* **2020**, *8*, 1019. [CrossRef]

38. Jiang, Z.; Zhang, J.; Nie, Z.; Guo, Z.; Zhu, L.; Cong, W.; Chen, Y.; Liang, Z. The Application of Seabed Silt in the Preparation of Artificial Algal Reefs. *Appl. Sci.* **2020**, *10*, 7279. [CrossRef]

39. Yu, D.Y.; Zhao, W.; Wang, F.Y. Trapezoid artificial reefs in different deployment spacing: Physical and numerical simulations. *Oceanol. Limnol. Sin.* **2020**, *51*, 283–292. [CrossRef]

40. Guan, C.T.; Li, M.J.; Zheng, Y.X.; Sun, L.; Nie, Z.; Wang, J.; Xie, W.; Jiang, Z. Numerical simulation of disposal space and analysis on physical stability of three-tube artificial reefs. *Period. Ocean. Univ. China* **2016**, *46*, 770. [CrossRef]

41. Pang, Y.X.; Li, F.C.; Li, Y. Study on three-dimensional numerical simulation of flow field effect of multi-aperture artificial fish reef under identical penetration rate. *J. Water Resour. Water Eng.* **2017**, *28*, 1802. [CrossRef]

42. Scarano, F. Tomographic PIV: Principles and practice. *Meas. Sci. Technol.* **2013**, *24*, 28. [CrossRef]

43. Christensen, K.T.; Scarano, F. Uncertainty quantification in particle image velocimetry. *Meas. Sci. Technol.* **2015**, *26*, 070201. [CrossRef]

44. Markus, R.; Jurgen, K.; Wereley, S.T.; Willert, C.E. Particle image velocimetry: A practical guide. *Exp. Fluid Mech.* **2017**, *255*, 160–162.

45. Rubinato, M.; Seungsoo, L.; Martins, R.; Shucksmith, J. Surface to sewer flow exchange through circular inlets during urban flood conditions. *J. Hydroinf.* **2018**, *20*, 564–576. [CrossRef]

46. Martins, R.; Rubinato, M.; Kesserwani, G.; Leandro, J.; Djordjevic, S.; Shucksmith, J. On the characteristics of velocity fields on the vicinity of manhole inlet grates during flood events. *Water Resour. Res.* **2018**, *54*, 6408–6422. [CrossRef]

47. Beg, M.d.N.A.; Carvalho, R.F.; Tait, S.; Brevis, W.; Rubinato, M.; Schellart, A.; Leandro, J. A comparative study of manhole hydraulics using stereoscopic PIV and different RANS models. *Water Sci. Technol.* **2017**, *1*, 87–98. [CrossRef]

48. Rojas, S.; Rubinato, M.; Nichols, A.; Shucksmith, J. Cost effective measuring technique to simultaneously quantify 2D velocity fields and depth-averaged solute concentrations in shallow water flows. *J. Flow Meas. Instrum.* **2018**, *64*, 213–223. [CrossRef]

49. Li, J.; Zheng, Y.X.; Gong, P.H.; Guan, C.T. Numerical simulation and PIV experimental study of the effect of flow fields around tube artificial reefs. *Ocean. Eng.* **2017**, *134*, 96–104.

50. Liu, Y.; Guan, C.T.; Zhao, Y.P.; Cui, Y.; Dong, G.H. Numerical Simulation and PIV Study of Unsteady Flow Around Hollow Cube Artificial Reef with Free Water Surface. *Eng. Appl. Comput. Fluid Mech.* **2012**, *6*, 527–540. [CrossRef]

51. Cui, Y.; Guan, C.T.; Wan, R.; Li, J. Numerical simulation on influence of disposal space on effects of flow field around artificial reefs. Trans. *Oceanol. Limnol.* **2011**, *41*, 40–48. [CrossRef]

52. Liu, J.; Jianzheng, W.U.; Jun, L.I.; Zhao, J.; Wang, L.; Zhang, W. Study of Tidal Current Characteristics in the Western Liaodong Bay. *Mar. Geol. Front.* **2015**, *31*, 10–17. [CrossRef]

53. Qian, Z.; Wang, M.; Ding, D.; Chen, W. Study on Hydrodynamic Characteristics in the Eastern Part of Liaodong Bay Mouth Based on Long-Term Observation. *Haiyang Xuebao* **2016**, *38*, 20–30.

54. Zhang, X.; Gang, S.; Qian, A.Z. Numerical Simulation of Tides and Tidal Currents in Liaodong Bay Based on Fvcom. Available online: https://en.cnki.com.cn/Article_en/CJFDTotal-HYFB201203021.htm (accessed on 5 October 2021).

55. Zhao, Q.; Chen, C.; Ding, D.; Chen, W. Study on Coastal Current Characteristics in the Eastern Area of Liaodong Bay Based on the Observed Data from Seabed Based Platform. *Ocean. Eng.* **2016**, *34*, 118–124.

56. Zheng, Y.X.; Liang, Z.L.; Guan, C.T. Numerical simulation and experimental study on flow field of artificial reefs in three tube-stacking layouts. *Oceanol. Limnol. Sin.* **2014**, *45*, 11–19. [CrossRef]

57. Yu, C.D.; Yu, C.G.; Yan, S.Q. Hydrodynamic simulation to the best layout of artificial ship-reefs. *Oceanol. Limnol. Sin.* **2004**, *35*, 299–305.

58. Shuiabi, E.; Thomson, V.; Bhuiyan, N. Entropy as a measure of operational flexibility. *Eur. J. Oper. Res.* **2005**, *165*, 696–707. [CrossRef]

59. Pan, L.Z.; Lin, J.; Zhnag, S.Y. A numerical experiment of the effects of artificial reef on vertical 2-dimensional steady flow field. *J. Shanghai Fish. Univ.* **2005**, *9*, 770. [CrossRef]

60. Lin, S.-K. Classical and Statistical Thermodynamics. Ashley H. Carter. *Entropy* **2002**, *4*, 165–167. [CrossRef]

61. Zhu, Z.; Zhang, Y.; Gou, L.; Pang, B. An Entropic Approach to Estimating the Instability Criterion of People in Floodwaters. *Entropy* **2021**, *23*, 74. [CrossRef]

62. Li, G.; Shuang, F.; Zhao, P.; Le, C. An Improved Butterfly Optimization Algorithm for Engineering Design Problems Using the Cross-Entropy Method. *Symmetry* **2019**, *11*, 1049. [CrossRef]

63. Zhang, M.; Zhou, J.; Zhou, R. Evaluating Sustainability of Regional Water Resources Based on Improved Generalized Entropy Method. *Entropy* **2018**, *20*, 715. [CrossRef]

64. Al-Kouz, W.; Al-Muhtady, A.; Owhaib, W.; Al-Dahidi, S.; Hader, M.; Abu-Alghanam, R. Entropy Generation Optimization for Rarified Nanofluid Flows in a Square Cavity with Two Fins at the Hot Wall. *Entropy* **2019**, *21*, 103. [CrossRef]

65. Xiao, M.-X.; Lu, C.-H.; Ta, N.; Jiang, W.-W.; Tang, X.-J.; Wu, H.-T. Application of a Speedy Modified Entropy Method in Assessing the Complexity of Baroreflex Sensitivity for Age-Controlled Healthy and Diabetic Subjects. *Entropy* **2019**, *21*, 894. [CrossRef]

66. Hsieh, N.-K.; Lin, W.-Y.; Young, H.-T. High-Speed Spindle Fault Diagnosis with the Empirical Mode Decomposition and Multiscale Entropy Method. *Entropy* **2015**, *17*, 2170–2183. [CrossRef]

67. Kim, S.; Kim, Y.; Kang, N.; Kim, H.S. Application of the Entropy Method to Select Calibration Sites for Hydrological Modeling. *Water* **2015**, *7*, 6719–6735. [CrossRef]

68. Yonamoto, Y. Application of Maximum Entropy Method to Semiconductor Engineering. *Entropy* **2013**, *15*, 1663–1689. [CrossRef]

69. Ding, L.; Shao, Z.; Zhang, H.; Xu, C.; Wu, D. A Comprehensive Evaluation of Urban Sustainable Development in China Based on the TOPSIS-Entropy Method. *Sustainability* **2016**, *8*, 746. [CrossRef]

70. Reis, B.; van der Linden, P.; Sousa Pinto, I.; Almada, E.; Borges, M.T.; Hall, A.E.; Stafford, R.; Herbert, R.J.; Lobo-Arteaga, J.; Gaudêncio, M.J.; et al. Artificial Reefs in the North-East Atlantic Area: Present Situation, Knowledge Gaps and Future Perspectives. *Preprints* **2021**, 2021010238. [CrossRef]

71. Komyakova, V.; Chamberlain, D.; Jones, G.P.; Swearer, S.E. Assessing the performance of artificial reefs as substitute habitat for temperate reef fishes: Implications for reef design and placement. *Sci. Total. Environ.* **2019**, *668*, 139–152. [CrossRef] [PubMed]

72. Vivier, B.; Dauvin, J.C.; Navon, M.; Rusig, A.M.; Mussio, I.; Orvain, F.; Boutouil, M.; Claquin, P. Marine artificial reefs, a meta-analysis of their design, objectives and effectiveness. *Glob. Ecol. Conserv.* **2021**, *27*, e01538. [CrossRef]

73. Rubinato, M.; Luo, M.; Zheng, X.; Pu, J.H.; Shao, S. Advances in Modelling and Prediction on the Impact of Human Activities and Extreme Events on Environments. *Water* **2020**, *12*, 1768. [CrossRef]

74. Rubinato, M.; Nichols, A.; Peng, Y.; Zhang, J.; Lashford, C.; Cai, Y.; Lin, P.; Tait, S. Urban and river flooding: Comparison of flood risk management approaches in the UK and China and an assessment of future knowledge needs. *Water Sci. Eng.* **2019**, *12*, 274–283. [CrossRef]